

Quadratic Scaling Multireference Correlation in Long Molecules with the Density Matrix Renormalization Group

Johannes Hachmann, Wim Cardoen, and Garnet Kin-Lic Chan

*Department of Chemistry and Chemical Biology,
Cornell University, Ithaca, NY 14853-1301, USA*

(Dated: February 8, 2020)

We have devised and implemented a local *ab initio* Density Matrix Renormalization Group (DMRG) algorithm to describe multireference nondynamic correlations in large systems. For long molecules that are extended in one of their spatial dimensions, this method allows us to obtain an exact characterisation of correlation, in the given basis, with a cost that scales only quadratically with the size of the system. The reduced scaling is achieved solely through integral screening and without the construction of correlation domains. We demonstrate the scaling, convergence, and robustness of the algorithm in polyenes and hydrogen chains. We converge to exact correlation energies (with $1\text{-}10\mu E_h$ precision) in all cases and correlate up to 100 electrons in 100 active orbitals. We further use our algorithm to obtain exact energies for the metal-insulator transition in hydrogen chains and compare and contrast our results with those from conventional quantum chemical methods.

I. INTRODUCTION

The electronic structure of a chemical system features two types of electron correlation. The first is *nondynamic* correlation. This is associated with the correlation of electrons in nearly degenerate valence orbitals. The correct description of nondynamic correlation is necessary to establish the qualitative features of chemical bonding. The second is *dynamic* correlation. This is associated with excitations from valence degrees of freedom into the many non-bonding orbitals. The multiple weak excitations are responsible for establishing the detailed, quantitative structure of the electronic wavefunction.

In general, a correct description of strong nondynamic correlation in large systems is very difficult to obtain. When nondynamic correlation is important (e.g. during bond breaking), a single determinant or electronic configuration does not provide the correct qualitative structure of the wavefunction. Instead, the delicate balance in the valence degrees of freedom between the kinetic energy, which favours delocalisation, and the Coulomb energy, which favours localisation, results in competing electronic configurations and the correct electronic structure contains contributions from multiple determinants with significant weights. Complete-Active-Space Self-Consistent-Field (CASSCF) theories [1] correctly describe this type of structure by expanding the wavefunction in the complete space of the optimised valence (or “active”) degrees of freedom, but do so at the cost of a factorial scaling with the number of active electrons. Such calculations with more than $O(10)$ electrons remain extremely difficult at this time. Despite the impressive progress in local Generalised Valence Bond and Coupled Cluster (CC) Theories (e.g. [2, 3, 4, 5, 6, 7, 8, 9, 10, 11, 12, 13, 14]) which provide some capacity to break e.g. single bonds, such approaches do not possess the flexibility of a true multireference theory. The fundamental challenge therefore remains to find a multireference electronic structure method that is sufficiently flexible to correctly describe nondynamic correlation, yet which exhibits a non-

factorial scaling, and can thus be applied to large systems.

In this work, we will adopt the more modest goal of answering the question of how to describe nondynamic correlation in systems which are large in only one out of their three spatial extents. In quasi-one-dimensional systems the physics, that is familiar from three-dimensions, is notably modified. This is illustrated by the organic electronic materials (e.g. conjugated organic polymers and carbon nanotubes) which exhibit unusual interacting electron effects, arising from collective, domino-like correlations due to the coupled quasi-one-dimensional motions of many electrons along their conjugated π -backbone. As a simple example, in linear polyenes, electron-electron interactions contribute to make the lowest excited singlet state (the 2^1A_g state) one of double-excitation nature, rather than the singly excited HOMO \rightarrow LUMO state as one would expect in a single particle picture [15, 16, 17]. A more extreme example of this occurs in metallic nanotubes at low temperatures, where at low energies there are no singly excited states; all low-energy excitations are of collective nature, and the qualitative electronic structure is of Luttinger liquid form [18, 19, 20].

Here we demonstrate that the Density Matrix Renormalization Group (DMRG), which we and others have recently been investigating in quantum chemistry [21, 22, 23, 24, 25, 26, 27, 28, 29, 30, 31, 32, 33, 34, 35, 36, 37, 38, 39, 40, 41], provides a solution to the question above of how to flexibly and efficiently describe nondynamic correlation in systems that are large in one of their three spatial dimensions. Our analysis shows that the DMRG behaves as a local, multireference, size-consistent/size-extensive, and variational theory. From the intrinsic locality of the DMRG ansatz we formulate a DMRG algorithm, denoted for convenience as LDMRG, that scales only *quadratically* with the size of the system, without any need for an artificial imposition of orbital domains. The multireference nature of the ansatz also eliminates any need for separately localised occupied and virtual orbitals. Using this algorithm, we carry out numerically

exact DMRG calculations for long molecules, including polyenes in the π -active space and metallic and insulating hydrogen chains where we correlate up to 100 active electrons in 100 active orbitals.

The structure of our discussion is as follows. We first introduce the DMRG wavefunction ansatz in section II. Here we discuss its multireference, size-consistent and size-extensive, variational, and local properties, and the implications for the design of a local DMRG algorithm. In section III we show how a simple screening of integral amplitudes results in a robust and naturally quadratic-scaling DMRG algorithm. In section IV we present calculations on hydrogen molecular chains and polyenes in the π -active space and demonstrate the size-extensivity, computational scaling, and convergence of the LDMRG algorithm. As a difficult test of nondynamic correlation, we further carry out calculations on the metal-insulator transition in hydrogen chains for both symmetric and asymmetric bond stretching, and compare our results against existing quantum chemical methods (section V). Finally, our conclusions are presented in section VI.

II. THE DMRG ANSATZ

A. DMRG and Matrix Product States

In previous work [29], we have described the Renormalization Group formulation of the DMRG algorithm. However, as related by Östlund and Rommer [42, 43], and subsequently developed by other authors (see e.g. [44, 45]), the DMRG is also fruitfully analysed from the viewpoint of the underlying wavefunction ansatz, the Matrix Product State (MPS). Such a formulation will be convenient for our present discussion and we will recall the main points below; for a full presentation, we refer the reader to the excellent review by Schollwöck [45].

Consider an N -particle system in a state $|\Psi\rangle$ spanned by k orbitals. In occupation number representation, $|\Psi\rangle$ can be expanded as

$$|\Psi\rangle = \sum_{n_1 n_2 \dots n_k} \psi_{n_1 n_2 \dots n_k} |n_1 n_2 \dots n_k\rangle \quad (\text{II.1})$$

where $n_i = 0, 1$; $\sum_i n_i = N$. We now decompose the high dimensional coefficient tensor ψ into a chained matrix product via repeated singular value decompositions (SVD). For example, if there are only two orbitals, a singular value decomposition yields

$$\psi_{n_1 n_2} = \sum_i R_i^{n_1} \sigma_i R_i^{n_2} \quad (\text{II.2})$$

where \mathbf{R}^{n_1} and \mathbf{R}^{n_2} are the singular vectors and σ are the singular values. Similarly, for three orbitals, $\psi_{n_1 n_2 n_3}$ can

be decomposed via two singular value decompositions as

$$\begin{aligned} \psi_{n_1 n_2 n_3} &= \sum_i R_i^{n_1} \sigma_i S_i^{n_2 n_3} \\ &= \sum_{ij} R_i^{n_1} \sigma'_i R_{ij}^{n_2} R_j^{n_3} \end{aligned} \quad (\text{II.3})$$

where in the SVD of \mathbf{S}_i , all singular values have modulus one, since \mathbf{S}_i is an orthogonal matrix. In this way, through repeated SVDs, the k -dimensional coefficient tensor can be decomposed as a chain of matrix products,

$$\psi_{n_1 n_2 \dots n_k} = \text{Tr} \{ \mathbf{R}^{n_1} \mathbf{R}^{n_2} \dots \sigma \dots \mathbf{R}^{n_k} \}. \quad (\text{II.4})$$

So far the decomposition is exact since the \mathbf{R} matrices are full rank and will grow increasing large as the number of orbitals grows.

The *Matrix Product State* which underlies the DMRG algorithm, arises by truncating the maximum dimension of the matrices to be at most $M \times M$, and thus with this restriction, we write the MPS as

$$|\Psi\rangle = \sum_{n_1 n_2 \dots n_k} \text{Tr} \{ \mathbf{R}^{n_1} \mathbf{R}^{n_2} \dots \sigma \dots \mathbf{R}^{n_k} \} |n_1 n_2 \dots n_k\rangle. \quad (\text{II.5})$$

We now establish the relationship between the MPS and the usual formulation of the DMRG algorithm. Recall that any point in a DMRG sweep, the orbitals are partitioned into two blocks: a left block (spanning orbitals $1, \dots, f$ say) and a right block (spanning orbitals $g = f + 1, \dots, k$). Through successive renormalisation transformations we obtain an adaptive many-body basis of dimension M to span the orbitals $1, \dots, f$; let us denote these many-body states by $|l_f\rangle$. First we enlarge the left block by adding the next orbital to give a superblock with an associated space $\{|l_f\rangle\} \otimes \{|n_g\rangle\}$. Next we renormalise this space to form a new many-body basis $\{|l_g\rangle\}$ for the enlarged block spanning orbitals $1, \dots, g$, as

$$|l_g\rangle = \sum_{f n_g} R_{gf}^{n_g} |l_f n_g\rangle \quad (\text{II.6})$$

where the rows of the matrix \mathbf{R}^{n_g} are the M eigenvectors of the density matrix of the superblock $1, \dots, g$. After successive renormalisations, we see that the renormalised states take on a matrix product form, e.g.

$$\begin{aligned} |l_h\rangle &= \sum_{g n_h} R_{hg}^{n_h} |l_g n_h\rangle \\ &= \sum_{f g n_g n_h} R_{hg}^{n_h} R_{gf}^{n_g} |l_f n_g n_h\rangle \\ &= \dots \end{aligned} \quad (\text{II.7})$$

where each \mathbf{R}^{n_i} matrix is truncated to have maximum dimension $M \times M$.

To complete the identification of the underlying DMRG wavefunction with the Matrix Product State,

we introduce the corresponding renormalised many-body states $|r_g\rangle$ which span the orbitals $g = f + 1, \dots, k$. In the tensor-product space of the left and right blocks, we can write the full wavefunction in the form

$$|\Psi\rangle = \sum_{l_f r_g} \psi_{l_f r_g} |l_f r_g\rangle. \quad (\text{II.8})$$

Performing an SVD, we obtain

$$|\Psi\rangle = \sum_f |\bar{l}_f\rangle \sigma_f |\bar{r}_f\rangle. \quad (\text{II.9})$$

Substituting in the matrix product decomposition of the DMRG many-body basis for the left and right block basis states from (II.7) in eqn. (II.9) we identify the DMRG wavefunction with the Matrix Product State (II.5). Consequently, the DMRG can be viewed as a self-consistent optimisation algorithm for the Matrix Product State where the renormalisation matrices \mathbf{R}^{n_i} which parametrise the ansatz are determined one by one from the density matrices of the blocks, after each blocking step in a DMRG sweep. The number of retained states in the DMRG M thus coincides with the dimensionality of the matrices that parametrise the MPS. We note that the position of σ in the Matrix Product State corresponds to the point of division between left and right blocks in the DMRG algorithm. In principle, the DMRG wavefunction varies with different block partitionings along a sweep, but in practice, the variation is quite small.

B. DMRG as a local, multireference, variational, size-consistent ansatz for long systems

Starting from the perspective above, let us summarise some features of the DMRG/MPS ansatz.

1. Variational: Since we can associate a wavefunction with any DMRG block configuration, and a DMRG energy is evaluated as an expectation value of such a wavefunction, the energies appearing in the DMRG procedure are strictly variational.
2. Multireference: It is clear that the Hartree-Fock reference has no special significance in the DMRG state, and in particular, we do not order or rank excitations relative to a single reference state. Furthermore, in contrast to selected Configuration Interaction (CI) theories, none of the coefficients of expansion $\psi_{n_1 n_2 \dots n_k}$ are restricted to be zero.
3. Size-consistency: Within a physical ordering of the orbitals on the DMRG lattice, the Matrix Product State for two widely separated systems factorises into the product of Matrix Product States for each system separately. To see this, first arrange the orbitals into left and right blocks, with the left block containing orbitals of the first system,

and the right block containing orbitals of the second system. Since there is no coupling, the Matrix Product State for the total block configuration is a product $|\Psi\rangle = |l\rangle|r\rangle$, where $|l\rangle$ is a Matrix Product State for the first system considered alone (without changing the orbital ordering) and similarly for $|r\rangle$. Consequently, the DMRG energy is size-consistent.

4. Locality and compactness: The number of variational parameters in the Matrix Product State is $O(M^2 k)$ and its correlation length is determined by M . Thus in any system with a finite quantum (i.e. off-diagonal) correlation length along the DMRG lattice, we can obtain a given accuracy in the energy per unit site with *constant* M , independent of the size of the system. In such cases, for a given accuracy, the number of variational parameters in the DMRG scales linearly with the size of the molecule. The restriction to given M determines the finite correlation length that is captured by the ansatz; there is no need to *a priori* impose any orbital domains. Thus the DMRG is a naturally local scaling ansatz, and so long as the determination of the energy is also performed with an account of locality (e.g. through screening or multipole expansion) a low-order scaling correlation theory arises. Indeed this is the basis of the quadratic scaling algorithm in the next section. Note that a finite correlation length implies only that we are away from a quantum critical point; such wavefunctions need not be close to the Hartree-Fock reference in any sense, as is indeed the case for systems with strong interactions. Thus, the local correlation nature of the DMRG is different from that of other local correlation methods (such as local CCSD) since these require the *correction* to the mean-field reference to be small and to possess finite correlation length. The DMRG ansatz possesses a further technical advantage. Since no localisable Hartree-Fock reference is required, the favorable scaling of the DMRG is obtained in any local basis, and does not in particular need separate localisation in the occupied and virtual spaces. This is particularly advantageous when modelling correlated states which possess a shorter quantum correlation length than their parent mean-field reference (e.g. systems with small Hartree-Fock bandgaps), for which orbital localisation may be more difficult.
5. Long molecules: The Matrix Product State embodies a finite correlation length as measured along the DMRG orbital lattice, rather than as necessarily exists in the physical space. Consequently, we can only hold M constant as the system size increases - and obtain the same relative accuracy - if the locality in the physical system maps geometrically onto a one-dimensional lattice, i.e. the system is extended in only one of its three dimensions as in a long molecule and dynamic correlation

by means of large basis sets is avoided. If this is not the case, we will require M to scale exponentially in the size of the system to maintain accuracy, much like Full Configuration Interaction (FCI) or CASSCF theory. In practice, we have shown that with reasonable M we can still obtain highly accurate DMRG energies even in non-one-dimensional molecular systems with up to $O(40)$ active orbitals - i.e. to large to treat using FCI theory - but to model much larger extended non-one-dimensional networks of strongly interacting electrons, further progress in the DMRG method will be required.

III. A QUADRATIC SCALING PARALLELISED DMRG ALGORITHM

As described in the preceding section, in a quasi-one-dimensional system with a finite correlation length, the number of variational parameters required in the DMRG ansatz to achieve a given energy accuracy per unit site, is $O(M^2k)$. Since M , the number of DMRG states retained during the algorithm, is independent of system size, and k denotes the number of orbitals, $O(M^2k)$ is linear with system size. Thus so long as the evaluation of the energy and solution for the wavefunction parameters are carried out efficiently, we can obtain a low-order scaling DMRG algorithm.

The full computational scaling of a single DMRG sweep is $O(M^2k^4) + O(M^3k^3)$. Here, the $O(k^4)$ scaling arises in essence from the number of two electron integrals in the Hamiltonian H , written in second quantisation as

$$H = \sum_{ij} t_{ij} a_i^\dagger a_j + \sum_{ijkl} v_{ijkl} a_i^\dagger a_j^\dagger a_k a_l. \quad (\text{III.1})$$

To implement a quadratic scaling DMRG algorithm we need to work in a localised orthonormal basis, and screen the contributions from the two-electron integrals in the Hamiltonian. (Note we can use any localised orthonormal basis and we do not need to separately localise the occupied and virtual spaces as is commonly required in local correlation methods. For example, later in this work, we shall use the basis of overlap symmetrically orthonormalised atomic orbitals). As is well understood, in a large system described in a localised basis, the number of significant two-electron integrals below a given threshold scales only quadratically as non-classical Coulomb integrals i.e. integrals of the form $v_{ijkl} = \frac{1}{2}(i(1)l(1)|j(2)k(2))$ where $i(1), l(1)$ or $j(2), k(2)$ functions are widely separated, vanish exponentially with the separation between i, l or j, k centres.

In the DMRG, we work with a number of intermediate combinations of operators on each of the blocks of orbitals which are subsequently combined to construct the full H [29, 31]. A DMRG sweep, consisting of $O(k)$ sweep iterations (each comprising a different block configuration), requires $O(M^2k^4) + O(M^3k^3)$ time, $O(M^2k^2)$

FIG. 1: Standard block configuration in DMRG. From left to right, L , \circ_L , \circ_R , R .



memory, and $O(M^2k^3)$ disk storage. These asymptotic costs originate from manipulating the two-index intermediate operators $A_{ij}, B_{ij}, P_{ij}, Q_{ij}$ on the various blocks:

$$A_{ij(\in \text{blk})}^{\text{blk}} = a_i a_j \quad (\text{III.2})$$

$$B_{ij(\in \text{blk})}^{\text{blk}} = a_i^\dagger a_j \quad (\text{III.3})$$

$$P_{ij(\notin \text{blk})}^{\text{blk}} = \sum_{kl \in \text{blk}} v_{ijkl} a_k a_l \quad (\text{III.4})$$

$$Q_{ij(\notin \text{blk})}^{\text{blk}} = \sum_{kl \in \text{blk}} x_{ijkl} a_k^\dagger a_l \quad (\text{III.5})$$

$$x_{ijkl} = v_{ijkl} - v_{jikl} - v_{ijlk} + v_{jilk}. \quad (\text{III.6})$$

To begin, we employ screening to determine a set of significant two index operators that must be considered on each block, according to the following criterion:

$$\begin{aligned} A_{ij(\in \text{blk})}^{\text{blk}} &\text{discard if } v_{ijkl} < \text{thresh}_1 \text{ for all } kl \in \text{blk} \\ B_{ij(\in \text{blk})}^{\text{blk}} &\text{discard if } x_{ijkl} < \text{thresh}_1 \text{ for all } kl \in \text{blk} \\ P_{ij(\notin \text{blk})}^{\text{blk}} &\text{discard if } v_{ijkl} < \text{thresh}_1 \text{ for all } kl \in \text{blk} \\ Q_{ij(\notin \text{blk})}^{\text{blk}} &\text{discard if } x_{ijkl} < \text{thresh}_1 \text{ for all } kl \in \text{blk}. \end{aligned} \quad (\text{III.7})$$

In a DMRG block configuration, there are four kinds of blocks: the left block L , an orbital to be blocked with the left block \circ_L , an orbital to be blocked with the right block \circ_R , and the right block R (Fig. 1). Without screening, the number of two-index operators that must be considered on each block is $O(k^2)$, but in each case this is reduced to $O(k)$ after screening since eqns. (III.7) require centres i, j to be close in space. Since the number of operators is reduced, we also reduce the memory cost to $O(M^2k)$ per sweep iteration (block configuration). The disk usage is reduced to $O(M^2k^2)$ per sweep.

Next, we consider the computational costs of the different manipulations involving the two index operators in each of the three stages of a sweep iteration: (1) blocking, (2), solving for the wavefunction, and (3) decimation:

1. *Blocking*: Here we construct representations of the operators in the tensor product space of a large block and an additional orbital; for concreteness, we take the large block as the left block L , and the additional orbital as \circ_L , and we consider the operator P_{ij} . First, we accumulate $P_{ij}^L, P_{ij}^{\circ_L}$ in the new space $\{L\} \otimes \{\circ_L\}$; for each such term, the accumulation requires $O(M^2)$ time. Since there are $O(k)$ screened P_{ij} operators on both blocks L and

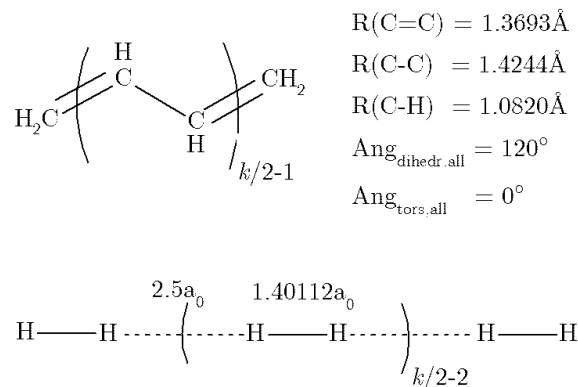
\circ_L , in total this requires $O(M^2k)$ time per blocking step and thus $O(M^2k^2)$ time per sweep. Next, we sum over the new terms appearing in eqns. (III.2), (III.3) that arise from the combinations $k \in L, l \in \circ_L$ and $k \in \circ_L, l \in L$; each such term requires $O(M^2)$ time per blocking step. Without screening the number of new terms become $O(k)$, but with screening we discard any contributions where $v_{ijkl} < \text{thresh}_2$ for all $kl \in \text{blk}$ and this decreases the number of new terms to $O(1)$ for each significant P_{ij} operator per blocking step. Consequently, the time to accumulate the additional contributions is $O(M^2) \times O(1) \times \text{no. significant } P_{ij} = O(M^2k)$ per blocking step, or $O(M^2k^2)$ time per sweep. Repeating this analysis for the A_{ij}, B_{ij}, Q_{ij} operators, we observe that these also involve $O(M^2k^2)$ time per sweep.

2. *Solving for the wavefunction:* In an iterative Davidson algorithm [46], the contributions of P_{ij}, Q_{ij} to the Hamiltonian matrix multiply takes the form $\sum_{ij} (P_{ij}^{L \circ L} \otimes A_{ij}^{\dagger \circ R R}) |\Psi\rangle, \sum_{ij} (Q_{ij}^{L \circ L} \otimes B_{ij}^{\circ R R}) |\Psi\rangle$. Each \otimes requires $O(M^3)$ time, and thus the overall cost is determined by the number of ij indices to sum over. From the screening criterion thresh_1 , this is $O(k)$ for each block configuration, and thus the total time for a single Hamiltonian multiply takes $O(M^3k)$, or $O(M^3k^2)$ per sweep.
3. *Decimation:* In the decimation for each two index operator, each transformation takes $O(M^3)$ time. After screening, only $O(k)$ ij indices need be considered per block, and thus the time to transform all $A_{ij}, B_{ij}, P_{ij}, Q_{ij}$ operators is $O(M^3k)$ per renormalisation step, or $O(M^3k^2)$ per sweep.

In summary, from the above analysis, integral screening in the LDMRG reduces the total computation cost per sweep to $O(M^3k^2) + O(M^2k^2)$ time (i.e. quadratic scaling, since M in long molecules is independent of system size for a chosen accuracy and hence a constant), $O(M^2k)$ memory, and $O(M^2k^2)$ disk. Table I summarises the key operations and costs of the screened algorithm. We note that we can also introduce screening for operators other than the two index operators in the DMRG. We have not done so here since this will not affect the asymptotic scaling.

Finally, we note that the above screening procedure is easily combined with the parallelised algorithm employed in our previous calculations [31]. Once the list of screened ij indices is determined via eqns. III.7, the significant operators are distributed over the processors, and all manipulations involving these operators are then carried out in parallel. This screened parallelised algorithm has been employed to perform the calculations described in the current work.

FIG. 2: Geometries of chemical systems used in the LDMRG study in sec. IV.



IV. NUMERICAL ANALYSIS OF THE LDMRG IN LONG SYSTEMS

In the current section, we report our numerical investigations of (i) the accuracy and extensivity of the LDMRG ansatz in long molecules, (ii) computational performance of the quadratic-scaling algorithm and robustness of the screening criteria, (iii) convergence of the LDMRG ansatz, and (iv) errors compared against standard correlation methods. We have chosen two classes of systems as representative “long” molecules: planar all-trans-polyenes C_kH_{k+2} ranging from $k = 4, 8, \dots, 48$ (modelled in the π_z -active space) and hydrogen molecule chains $(\text{H}_2)_{k/2}$ ranging from $k = 10, 20, \dots, 100$. The geometries of the polyenes (based on [47]) and hydrogen chains are given in fig. 2. We note that although the bond-lengths in the hydrogen molecule chains are alternating, the molecules are still spaced sufficiently closely to be interacting.

A. Computational details

All electronic integrals were obtained using the PSI3.2 package [48]. We used an STO-3G minimal basis for the polyene calculations and an STO-6G minimal basis for the hydrogen molecular chains [49, 50]. Polyene calculations were performed in the π_z -active space spanned by one p_z orbital on each carbon center, with each carbon atom contributing one electron; thus in C_kH_{k+2} we used a (k, k) active space. The remaining electrons were placed in doubly occupied Restricted Hartree-Fock (RHF) orbitals generated by the PSI3.2 program. Calculations on the hydrogen chains correlated all electrons.

We used an orthonormal basis as input to the LDMRG calculations, and furthermore, for the quadratic scaling algorithm, we require this basis to be localised. In both the polyenes and hydrogen chains we obtained a localised orthonormal basis by symmetrically orthonormalising ($S^{-1/2}$) the atomic orbital basis. The orthonormalised orbitals were then ordered in their natural topo-

TABLE I: Time, memory, and disk costs associated with the two-index operators in the original DMRG and screened LDMRG algorithms. The two-index operators determine the asymptotic computational costs of the algorithm.

Operator	Blocking		Solving		Decimation		Memory		Disk	
	DMRG	LDMRG	DMRG	LDMRG	DMRG	LDMRG	DMRG	LDMRG	DMRG	LDMRG
A_{ij}, B_{ij}	M^2k^3	M^2k^2	M^3k^3	M^2k^2	M^3k^3	M^3k^2	M^2k^2	M^2k	M^2k^3	M^2k^2
P_{ij}, Q_{ij}	M^2k^4	M^2k^2	M^3k^3	M^2k^2	M^3k^3	M^3k^2	M^2k^2	M^2k	M^2k^3	M^2k^2

logical order i.e. in the order of their originating atoms along the chain. Since each atom contributes only one basis function, this ordering is unique.

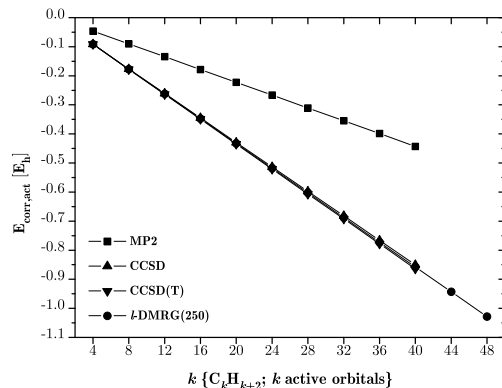
The LDMRG calculations were performed with the parallel BLOCK code [31] with integral screening as described in sec. III, on 4-18 processors. Except where stated otherwise (see sec. IV C), we applied screening thresholds of $\text{thresh}_1 = 10^{-7}E_h$ and $\text{thresh}_2 = 10^{-20}E_h$. No spatial symmetry was used. DMRG sweeps were performed with progressively increasing M values (a sweep schedule) and a small amount of random noise (between $10^{-6} - 10^{-9}$ in the matrix norm) was added to the density matrix in the early sweeps ($M \leq 100$) to prevent loss of quantum numbers [29, 31]. A typical schedule to obtain $M = 50, 100, 250$ DMRG energies is as follows: sweeps 1-6: $M = 50$ (with noise), sweeps 7-12: $M = 50$, sweeps 13-18: $M = 100$ (with noise), sweeps 19-24: $M = 100$, sweeps 25-30: $M = 250$. We have converged our LDMRG energies to 8 significant figures; unconverged digits are denoted in italics. Because of the complexity of the ab initio DMRG method and the high non-linearity of the optimisation, there is a small dependence of the DMRG energies on the precise computational setup (e.g. the way in which M is increased in sweeps) which may lead to some variation in the last significant digit.

B. Accuracy and Extensivity of the DMRG ansatz

In Tables II and III we present the energies obtained with our quadratic scaling LDMRG algorithm for the all-trans-polyene series and hydrogen molecular chains. For comparison, we also present second-order Møller-Plesset (MP2) and Coupled Cluster calculations (CCSD, CCSD(T)) obtained using the Psi3.2 (hydrogen chains) and DALTON 2.0 [51] (active-space polyenes) packages.

In the largest M LDMRG calculations shown, the correlation energies are exact correlation energies for the many-particle Schrödinger equation to the digits displayed. For example, in the polyenes, calculations at the LDMRG(500) and LDMRG(1000) level did not change the energy in the μE_h -range. To confirm the exactness of our LDMRG calculations, we also performed explicit active space FCI calculations (using MOLPRO 2002.6 [52]) for C_4H_6 and C_6H_8 and obtained agreement to all displayed digits. Following the discussion in sec. IV A, the hydrogen molecular chain energies are presented to $10\mu E_h$ precision, corresponding to eight significant figures in the electronic energy of the longer chains. There

FIG. 3: All-trans-polyenes: Active space correlation energy from MP2, CCSD, CCSD(T) and LDMRG(250) as a function of polyene chain length. On the scale of the graph, the LDMRG and CC results nearly overlap.



are only improvements of the order of $1\mu E_h$ when going to LDMRG(100) and thus the LDMRG(50) correlation energies for the hydrogen molecular chains are exact to the digits displayed.

The largest Hilbert space considered (for the $(H_2)_{50}$ system containing 100 electrons in 100 orbitals) has $\dim(\mathcal{H})=10^{58}$. That we are able to obtain a numerically exact correlation energy with the LDMRG illustrates the compactness of the LDMRG description in systems that are still interacting but have finite correlation lengths, which allows us to keep M fixed as the system size grows (see sec. II A). A related feature of the LDMRG ansatz is that of size-consistency/extensivity of the energy, which we shall now discuss.

In fig. 3, we plot the active space correlation energy $E_{\text{corr,act}}$ as a function of polyene chain length. A clear linear relationship between chain length and correlation energy is observed. Fig. 4 shows in detail how the active space correlation energy as well as the total energy E_{tot} per additionally introduced C_4H_4 -unit converges to a constant in the limit of long polyenes.

We also performed a series of lower accuracy LDMRG calculations for the polyenes, with $M = 5 - 40$ states. Due to the variational nature of the DMRG, these approach the exact energy from above. Fig. 5 presents the logarithm of the percentage error in the correlation en-

FIG. 4: All-trans-polyenes: Exact (LDMRG(250)) total energy per additionally introduced C_4H_4 -unit. The inlay shows the active space correlation energy at CCSD, CCSD(T) and LDMRG(250) level of theory per additionally introduced C_4H_4 -unit.

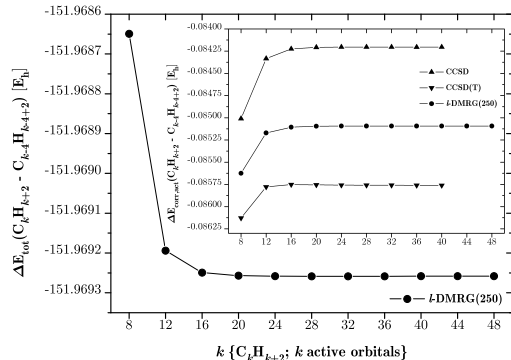
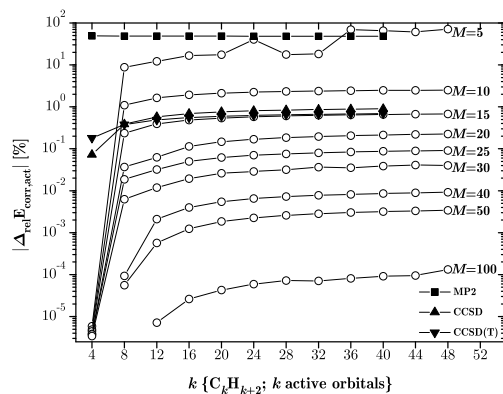


FIG. 5: All-trans-polyenes: Relative errors in the active space correlation energies for LDMRG with various M (compared to the exact LDMRG(250) results). The black marked curves are the errors of MP2, CCSD, and CCSD(T) as reference. The plot shows absolute magnitudes in logarithmic scale.



ergy relative to the "exact" LDMRG(250) energies, as a function of chain length. In small systems the LDMRG calculations are exact, since the DMRG states span the whole N -particle space. In the longer polyenes, the percentage errors increase to a saturating value, demonstrating the size-extensivity of the approximate LDMRG calculations. Similar observations can be made for the hydrogen molecular chains.

C. Computational Scaling and Screening Robustness

In Figure 6 we present the asymptotic computational scaling of the sweep time for the LDMRG calculations as a function of the number of active orbitals for the polyenes and hydrogen molecular chains. Here sweep times were measured after several sweeps at a given M level have been performed, to remove the bias that occurs immediately after a transition from a lower M calculation in the sweep schedule.

We fitted the timing data to obtain the computational scaling of LDMRG as a function of the number of active orbitals. The scaling exponents for the polyenes and the $(H_2)_{k/2}$ -chains with different M and screening thresholds are given in tab. V.

In the polyenes we find a reduced scaling of near-quadratic order, with an exponent between 2.1 – 2.2. For reasonable screening thresholds (i.e. $\text{thresh}_1 10^{-6}E_h - 10^{-8}E_h$) no significant differences in the scaling is observed. We also do not see a significant scaling dependence on M . In the hydrogen chains a similar reduced scaling was found, in this case with exponents ranging from 2.2 – 2.4. In both cases, it is clear that the screened LDMRG algorithm has reduced the computational scaling of the DMRG to quadratic order. As an example of absolute times per sweep, for the largest system $(H_2)_{50}$ using 18 2.0 GHz Opteron processors, we required 27min for $M = 50$, 37min for $M = 100$, and 73min for $M = 250$.

Since the LDMRG employs screening, we should assess the robustness of the criterion that is used. To this end, we studied the polyene correlation energies computed with screening thresholds (thresh_1) of $10^{-6}E_h$, $10^{-7}E_h$, $10^{-8}E_h$ and $10^{-20}E_h$ (the energy of the latter can be considered unscreened). A selection of results is presented in tab. IV. We observe the correlation energy to be converged at the μE_h level with respect to the screening threshold when $\text{thresh}_1 = 10^{-7}E_h$, which is the reason for using this setting during this study. In practice, this threshold could even be relaxed for lower accuracy calculations.

D. Sweep and Error Convergence

There are two types of convergence in DMRG calculations. The first is the convergence of the energy as a function of the number of sweeps, holding the number of DMRG states M fixed. We observed that on average, convergence was achieved in only 4–6 sweeps for small M and 2–4 sweeps for large M values (not inclusive of the noise sweeps and the preceding sweeps in the schedule).

The second type of convergence relates to the approach of the DMRG energy to the exact energy as the number of retained states M is increased. Here, we analyse our data for the DMRG calculations on polyenes with different M values. The precise analytic form of the DMRG energy convergence as a function of M has been a matter of

TABLE II: All-trans-polyenes: Dimension of the FCI determinant space, total RHF energy, RHF active space electronic energy; active space correlation energies at MP2, CCSD, CCSD(T) and different LDMRG levels of theory. All energies are given in hartrees.

Molecule	$\dim(\mathcal{H})^a$	E_{RHF}	$E_{\text{corr,act}}$									
			$E_{\text{RHF,el,act}}^b$		MP2	CCSD	CCSD(T)	LDMRG(50)	LDMRG(100)	LDMRG(250) ^c		
C ₄ H ₆	3.6×10^1	-153.006 364	-3.169 490	-0.046 529	-0.091 435	-0.091 668	-0.091 502	<i>conv.</i> ^d	<i>conv.</i>			
C ₈ H ₁₀	4.9×10^3	-304.889 389	-8.426 391	-0.090 346	-0.176 445	-0.177 797	-0.177 127	<i>conv.</i>	<i>conv.</i>			
C ₁₂ H ₁₄	8.5×10^5	-456.773 412	-14.589 838	-0.134 320	-0.260 779	-0.263 575	-0.262 296	-0.262 297	<i>conv.</i>			
C ₁₆ H ₁₈	1.7×10^8	-608.657 556	-21.345 452	-0.178 366	-0.345 003	-0.349 327	-0.347 399	-0.347 403	<i>conv.</i>			
C ₂₀ H ₂₂	3.4×10^{10}	-760.541 718	-28.542 181	-0.222 434	-0.429 210	-0.435 082	-0.432 490	-0.432 498	<i>conv.</i>			
C ₂₄ H ₂₆	7.3×10^{12}	-912.425 883	-36.090 721	-0.266 507	-0.513 414	-0.520 840	-0.517 579	-0.517 591	<i>conv.</i>			
C ₂₈ H ₃₀	1.6×10^{15}	-1064.310 048	-43.931 953	-0.310 582	-0.597 618	-0.606 599	-0.602 668	-0.602 684	<i>conv.</i>			
C ₃₂ H ₃₄	3.6×10^{17}	-1216.194 214	-52.023 816	-0.354 658	-0.681 822	-0.692 358	-0.687 757	-0.687 777	<i>conv.</i>			
C ₃₆ H ₃₈	8.2×10^{19}	-1368.078 379	-60.334 842	-0.398 734	-0.766 027	-0.778 118	-0.772 846	-0.772 870	<i>conv.</i>			
C ₄₀ H ₄₂	1.9×10^{22}	-1519.962 544	-68.840 593	-0.442 810	-0.850 231	-0.863 879	-0.857 935	-0.857 962	-0.857 963			
C ₄₄ H ₄₆	4.4×10^{24}	-1671.846 710	-77.521 543	<i>e</i>	<i>e</i>	<i>e</i>	-0.943 024	-0.943 055	-0.943 056			
C ₄₈ H ₅₀	1.0×10^{27}	-1823.730 875	-86.361 727	<i>e</i>	<i>e</i>	<i>e</i>	-1.028 113	-1.028 147	-1.028 149			

^a $\dim(\mathcal{H}) = \binom{k_\alpha}{N_\alpha} \binom{k_\beta}{N_\beta}$, i.e. here $\dim(\mathcal{H}) = \binom{k/2}{k/2}^2$. No point group symmetry used.

^bThe active space electronic energy contains the core-active Coulomb and exchange contributions, but no nuclear repulsion.

^cAll calculations with $M \geq 250$ converged.

^d"*conv.*" denotes converged results, where increased M did not change the significant figures in the energy.

^eC₄₄H₄₆ and C₄₈H₅₀ could not be computed by DALTON due to an address limitation.

TABLE III: (H₂)_{k/2}-chains: Dimension of the FCI determinant space, total RHF energy, RHF electronic energy; correlation energies at MP2, CCSD, CCSD(T) and LDMRG(50) levels of theory. All energies are given in hartrees.

Molecule	$\dim(\mathcal{H})^a$	E_{RHF}	$E_{\text{RHF,el}}$	E_{corr}				
				MP2	CCSD	CCSD(T)	LDMRG(50) ^b	
(H ₂) ₅	6.4×10^4	-5.553 26	-16.036 48	-0.068 34	-0.101 93	-0.102 04	-0.102 09	
(H ₂) ₁₀	3.4×10^{10}	-11.088 22	-38.784 11	-0.137 53	-0.203 77	-0.204 04	-0.204 15	
(H ₂) ₁₅	2.4×10^{16}	-16.623 18	-64.210 83	-0.206 72	-0.305 61	-0.306 03	-0.306 21	
(H ₂) ₂₀	1.9×10^{22}	-22.158 14	-91.378 72	-0.275 91	-0.407 44	-0.408 02	-0.408 26	
(H ₂) ₂₅	1.6×10^{28}	-27.693 11	-119.841 65	-0.345 10	-0.509 28	-0.510 01	-0.510 32	
(H ₂) ₃₀	1.4×10^{34}	-33.228 07	-149.336 70	-0.414 29	-0.611 12	-0.612 01	-0.612 38	
(H ₂) ₃₅	1.3×10^{40}	-38.763 03	-179.690 11	-0.483 48	-0.712 95	-0.714 00	-0.714 44 ^c	
(H ₂) ₄₀	1.2×10^{46}	-44.297 99	-210.778 35	-0.552 67	-0.814 79	-0.815 99	-0.816 49	
(H ₂) ₄₅	1.1×10^{52}	-49.832 95	-242.509 08	-0.621 87	-0.916 63	-0.917 98	-0.918 55	
(H ₂) ₅₀	1.0×10^{58}	-55.367 92	-274.810 58	-0.691 06	-1.018 47	-1.019 98	-1.020 61	

^aNo point group symmetry used.

^bAll calculations with $M \geq 50$ converged.

^cThis result lies very close on the rounding border, LDMRG(50) rounds the last digit to 4, LDMRG(100) to 5.

debate in the literature [26, 29, 36, 53, 54]. We have previously found good agreement with the proposed form of Okunishi et al. [53, 54],

$$\Delta E(M) \sim \exp[-\kappa (\log M)^\alpha], \quad \alpha = 2 \quad (\text{IV.1})$$

which is slower than exponential but still faster than algebraic. In fig. 7 we plot the logarithm of the percentage error in the correlation energy against $(\log M)^2$,

which shows a clear linear fit. By contrast, the inlay demonstrates that the error indeed does not decay exponentially. Fitting our data (omitting $M = 5$) to the general form of eqn. IV.1 we obtained an exponent of $\alpha \sim 1.6 - 1.8$. Fixing $\alpha = 2$, we obtain values between $\kappa = 1.80 \pm 0.03$ (for C₁₂H₁₄) and $\kappa = 1.45 \pm 0.03$ (for C₄₈H₅₀).

Corresponding to the rapid energy convergence we also

TABLE IV: All-trans-polyenes: Active space correlation energies from LDMRG(250) with screening thresholds $10^{-6}E_h$ and $10^{-7}E_h$; absolute and relative errors of $10^{-6}E_h$ -screening (compared to the exact results from $10^{-7}E_h$ -screening). All energies are given in hartrees.

Molecule	$E_{\text{corr,act}}$		Δ_{abs}	$\Delta_{\text{rel}} [\%]$
	$(10^{-6}E_h)$	$(10^{-7}E_h)$		
C_8H_{10}	-0.177 127	<i>conv.</i>	0	0
$C_{16}H_{18}$	-0.347 405	-0.347 404	-0.000 001	-0.46×10^{-5}
$C_{32}H_{34}$	-0.687 765	-0.687 777	0.000 008	1.52×10^{-5}
$C_{40}H_{42}$	-0.857 942	-0.857 963	0.000 021	3.01×10^{-5}
$C_{48}H_{50}$	-1.028 093	-1.028 149	0.000 056	6.41×10^{-5}

FIG. 6: $(H_2)_{k/2}$ -chains (circles) and all-trans-polyenes (squares): Asymptotic timing data (i.e. total time per sweep) of LDMRG with $M = 50$ (filled marks) and $M = 250$ (unfilled marks) for $10^{-7}E_h$ -screening in log-log-representation with linear fit.

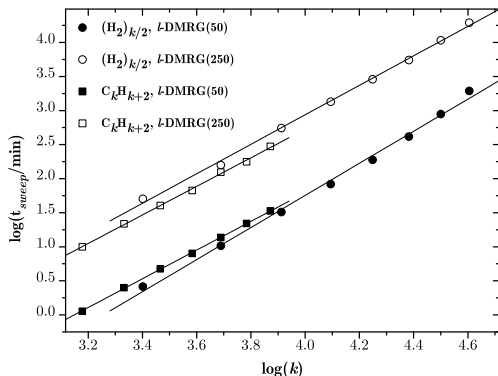
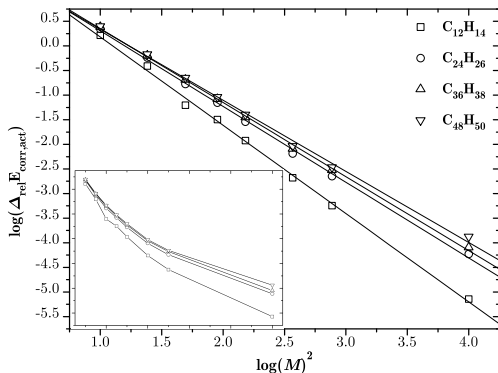


FIG. 7: All-trans-polyenes: Convergence of the relative errors in the active space correlation energies for LDMRG as a function of M (compared to the exact LDMRG(250) results). The main plot shows magnitudes in logarithmic scale over $\log(M)^2$ (with linear fit), the inlay shows them over $\log(M)$.



observed a rapid decrease of the truncated weight of the density matrix as M is increased. This shows that the local representation is well suited for the description of the chemical system and physical problem at hand [35, 45, 55].

E. Comparison with Perturbation and Coupled Cluster Theories

Since with our larger M LDMRG calculations we have exact energies at our disposal we can now analyze the errors at the various levels of theory in more detail.

In the polyene calculations (tab. II) the largest DMRG absolute error is $35\mu E_h$ for the $C_{48}H_{50}$ molecule at the $M = 50$ level. This corresponds to $\sim 10^{-3}\%$ of the exact active space correlation energy, and $\sim 10^{-5}\%$ of the exact total active space electronic energy. Compared to the Coupled Cluster errors, LDMRG(50) is already better by 2-3 orders of magnitude. The LDMRG(100) gives a further order of magnitude improvement, and is essentially exact. In our more approximate calculations (fig. 5) we find that LDMRG with $M = 10$ performs better than MP2, and with $M = 15$ better than CCSD and CCSD(T). The results for $M = 5$ are not reliable due to loss of important quantum numbers.

Surprisingly we observe that the CCSD(T) results lie below the exact energies computed with LDMRG. Despite CCSD(T) being nonvariational in general, it is still uncommon to not obtain an energy above the exact energy at an equilibrium geometry. In general the triples correction performed relatively badly for the polyenes. The CCSD(T) absolute errors show little improvement compared to CCSD, and for C_4H_6 it is even worse than CCSD.

In case of the hydrogen chains, the convergence of the LDMRG with M was more rapid and results were already exact with $M = 50$. CCSD(T) also performed better in this system, the triples correction improved on CCSD by $1/2$ order of magnitude, and the resulting energies were consistently above the exact energies.

We point out, that the DMRG allows to seamlessly adjust the desired accuracy without any change or extension of the implementation.

V. THE METAL-INSULATOR TRANSITION IN LINEAR HYDROGEN

As an example of a challenging electronic problem, we studied the symmetric and asymmetric bond stretching in a linear H_{50} -chain. In both these cases, the system transitions from a state with metallic correlations at compressed geometries to an insulating state with strong multireference correlation in the dissociation region. This bond breaking process is hence dominated by a varying nature of chemical bonding and electron correlation, with

TABLE V: Asymptotic scaling exponents (with standard error) of LDMRG depending on M and the screening threshold.

System (thresh ₁ [E _h])	Scaling exponent		
	LDMRG(50)	LDMRG(100)	LDMRG(250)
C _k H _{k+2} (10 ⁻⁶)	2.12±0.02	2.11±0.01	2.07±0.09
C _k H _{k+2} (10 ⁻⁷)	2.11±0.02	2.11±0.01	2.10±0.03
C _k H _{k+2} (10 ⁻⁸)	2.12±0.01	2.07±0.02	2.09±0.03
C _k H _{k+2} (10 ⁻²⁰)	3.27±0.08	3.33±0.10	3.53±0.06
(H ₂) _{k/2} (10 ⁻⁷)	2.36±0.06	2.18±0.05	2.16±0.04

which an electronic structure method has to effectively cope.

In case of the symmetric dissociation we begin with a uniform bond-distance between all H-atoms of $R=1.0a_0$, and stretch all 49 bonds symmetrically and simultaneously to $R=1.2, 1.4, \dots, 4.2a_0$. The final structure consists of 50 equidistant, nearly-independent H-atoms on a line.

In case of the asymmetric dissociation we distinguish alternating bonds as intermolecular and intramolecular with R_{inter} and R_{intra} . The first geometry is $R_{\text{intra}}=R_{\text{inter}}=1.4a_0$. In the following geometries R_{intra} is kept fixed at $1.4a_0$ while R_{inter} grows to $R_{\text{inter}}=1.6, 1.8, \dots, 4.2a_0$. The final structure consists of 25 equidistant, nearly-independent H₂-molecules at equilibrium bond distance on a line.

We computed the electronic energy using the LDMRG (with up to 1000 states) in the minimal STO-6G basis, where we correlated all 50 electrons in 50 orbitals.

A. Symmetric Dissociation

The calculated energies for the symmetric dissociation are summarized in tab. VI. The potential energy curves at RHF, MP2, and exact LDMRG level of theory are plotted in fig. 8. It can immediately be seen how the contribution of correlation increases along the dissociation coordinate: In the dissociation limit the share of the correlation energy in the total energy grows to $\sim 20\%$ and in the electronic energy to $\sim 7\%$, which emphasizes the importance of nondynamic correlation in this problem.

As is expected, RHF and MP2 behave poorly as the chain dissociates. The Coupled Cluster energies cannot even be converged for bond lengths $R > 2.0a_0$. This is a fundamental problem in CC theory that is well documented e.g. in the work of Takahashi and Paldus and others [56, 57, 58] where in one-dimensional systems, even for physically relevant coupling parameters, the Coupled Cluster doubles equations may have no real solutions. The correlation energy errors for different methods relative to the exact LDMRG results are shown in Fig. 9.

It is understood that we need to retain more states in the LDMRG in the metallic regime if we start from a local atomic orbital basis, since we need to capture the delocalisation and long-range off-diagonal correlations [45]. We

FIG. 8: Symmetric dissociation of H₅₀: Potential energy curves from RHF, MP2, and exact LDMRG. On the scale of the graph, the few available CCSD and CCSD(T) datapoints were indistinguishable from the LDMRG data.

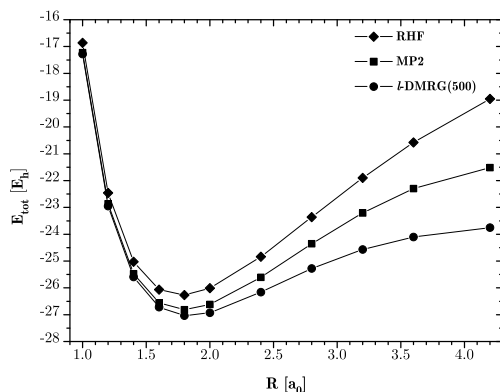


FIG. 9: Symmetric dissociation of H₅₀: Relative errors in the correlation energies at MP2, CCSD, CCSD(T), and different LDMRG levels of theory (compared to the exact LDMRG results) in logarithmic scale.

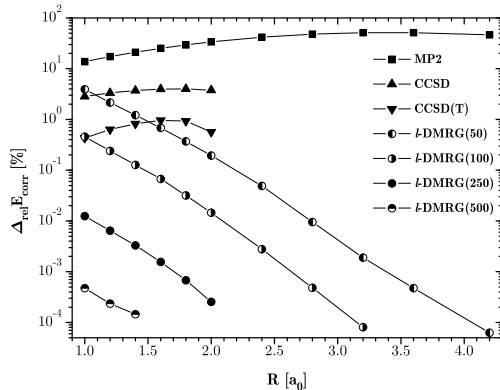


TABLE VI: Symmetric dissociation of H_{50} : Total RHF energy, RHF electronic energy; correlation energies at MP2, CCSD, CCSD(T) and various LDMRG levels of theory. All energies are given in hartrees.

R [a_0]	E_{RHF}	$E_{\text{RHF,el}}$	E_{corr}							
			MP2	CCSD	CCSD(T)	LDMRG(50)	LDMRG(100)	LDMRG(250)	LDMRG(500) ^a	
1.0	-16.864 88	-191.825 14	-0.361 45	-0.407 29	-0.417 39	-0.402 72	-0.417 27	-0.419 14	-0.419 19	
1.2	-22.461 27	-168.261 49	-0.401 83	-0.470 11	-0.483 30	-0.475 90	-0.485 21	-0.486 35	-0.486 38	
1.4	-25.029 76	-150.001 38	-0.444 73	-0.543 03	-0.559 36	-0.557 16	-0.563 30	-0.564 00	-0.564 02	
1.6	-26.062 25	-135.412 42	-0.491 88	-0.631 18	-0.650 89	-0.652 72	-0.656 74	-0.657 18	-0.657 19	
1.8	-26.265 98	-123.466 13	-0.545 50	-0.741 67	-0.765 47	-0.769 82	-0.772 42	-0.772 66	-0.772 67	
2.0	-26.008 20	-113.488 34	-0.607 89	-0.883 29	-0.912 70	-0.916 11	-0.917 76	-0.917 89	<i>conv.</i> ^b	
2.4	-24.835 76	-97.735 87	-0.768 83		<i>c</i>	<i>c</i>	-1.324 16	-1.324 77	-1.324 81	<i>conv.</i>
2.8	-23.360 81	-85.846 62	-0.995 30		<i>c</i>	<i>c</i>	-1.913 81	-1.913 98	-1.913 99	<i>conv.</i>
3.2	-21.896 33	-76.571 41	-1.307 78		<i>c</i>	<i>c</i>	-2.671 90	-2.671 95	<i>conv.</i>	<i>conv.</i>
3.6	-20.574 29	-69.174 36	-1.723 32		<i>c</i>	<i>c</i>	-3.528 46	-3.528 48	<i>conv.</i>	<i>conv.</i>
4.2	-18.955 95	-60.613 15	-2.558 99		<i>c</i>	<i>c</i>	-4.793 76	<i>conv.</i>	<i>conv.</i>	<i>conv.</i>

^aAll calculations with $M \geq 500$ converged.

^b"*conv.*" denotes converged results, where increased M did not change the significant figures in the energy.

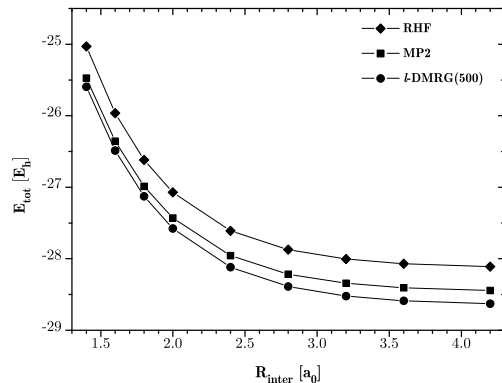
^cThe Coupled Cluster calculations could not be converged. See text.

find that both the convergence with the number of sweeps as well as with M is slower as compared to calculations in the nonmetallic regime. At $R=1.0a_0$ LDMRG(50) is worse than CCSD, LDMRG(100) slightly worse than CCSD(T), and for $R < 1.6a_0$ LDMRG(50) is still worse than CCSD(T). In the metallic region LDMRG required $M = 500$ to converge to the numerically exact result. In essence, by using orthonormalised atomic orbitals, we are starting from a particularly unfavourable one-particle basis to describe metallic behaviour. By performing the DMRG in a set of separately localised occupied and virtual orbitals such as Boys orbitals [59], we expect that the degradation in efficiency of the DMRG would be avoided.

B. Asymmetric Dissociation

The calculated energies for the asymmetric dissociation are summarized in table VII. In this system, the restricted Hartree-Fock reference dissociates correctly (to a set of non-interacting hydrogen molecules), which can be understood by changing to a localised basis in the space of restricted occupied orbitals. For this reason, the restricted MP2 and CC theories are also qualitatively correct and we see that their energies (fig. 10) lie parallel to the exact LDMRG values along the dissociation curve. Unlike in the symmetric dissociation, the correlation energy saturates rapidly to $\sim 1.8\%$ of the total energy as the bonds are stretched. Fig. 11 shows how the percentage errors in the correlation energy for the different methods decrease along the dissociation coordinate. Again, we see reduced performance of the DMRG in the metallic regime due to the unsuitability of the underlying orbital basis, but still a systematic convergence with M . For

FIG. 10: Asymmetric dissociation of H_{50} : Potential energy curves from RHF, MP2, and exact LDMRG. On the scale of the graph, the LDMRG, CCSD, and CCSD(T) curves are indistinguishable.



large R_{inter} we observed very rapid convergence with M and number of sweeps, and in fact for $R_{\text{inter}}=4.2a_0$ the LDMRG energy was already exact after 4 noise sweeps with $M = 50$. In the limit of complete dissociation, the CCSD theory becomes exact for the system at hand and this is confirmed by convergence to the LDMRG results.

In order to demonstrate the metal-insulator transition more explicitly we computed the one-particle reduced density matrix γ during our LDMRG calculations. In fig. 12 we have plotted the off-diagonal decay of the α one-particle density matrix from element $\gamma_{25,25} \rightarrow \gamma_{25,50}$. In the metallic regime (short R_{inter}) we see the long-ranged

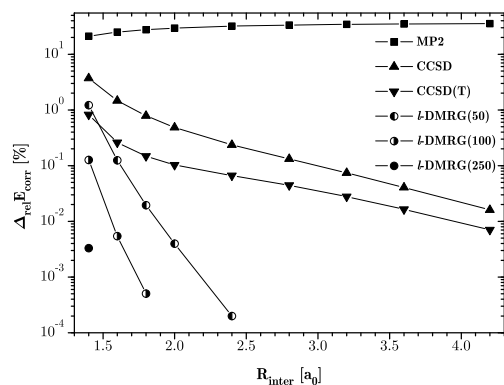
TABLE VII: Asymmetric dissociation of H_{50} : Total RHF energy, RHF electronic energy; correlation energies at MP2, CCSD, CCSD(T) and various LDMRG levels of theory. All energies are given in hartrees.

$R_{\text{inter}} [a_0]$	E_{RHF}	$E_{\text{RHF,el}}$	E_{corr}								
			MP2	CCSD	CCSD(T)	LDMRG(50)	LDMRG(100)	LDMRG(250)	LDMRG(500) ^a		
1.4	-25.029 76	-150.001 38	-0.444 73	-0.543 03	-0.559 36	-0.557 16	-0.563 30	-0.564 00	-0.564 02		
1.6	-25.963 71	-142.811 31	-0.392 61	-0.516 01	-0.522 30	-0.523 02	-0.523 64	-0.523 67	<i>conv.</i> ^b		
1.8	-26.617 68	-136.573 91	-0.369 20	-0.505 47	-0.508 73	-0.509 38	-0.509 48	<i>conv.</i>	<i>conv.</i>		
2.0	-27.071 82	-131.089 88	-0.357 01	-0.503 04	-0.504 97	-0.505 48	-0.505 50	<i>conv.</i>	<i>conv.</i>		
2.4	-27.609 24	-121.878 99	-0.346 20	-0.507 17	-0.508 03	-0.508 37	<i>conv.</i>	<i>conv.</i>	<i>conv.</i>		
2.8	-27.873 62	-114.445 23	-0.341 62	-0.512 77	-0.513 22	-0.513 45	<i>conv.</i>	<i>conv.</i>	<i>conv.</i>		
3.2	-28.004 68	-108.324 99	-0.338 67	-0.516 18	-0.516 42	-0.516 56	<i>conv.</i>	<i>conv.</i>	<i>conv.</i>		
3.6	-28.069 65	-103.203 54	-0.336 34	-0.517 50	-0.517 63	-0.517 71	<i>conv.</i>	<i>conv.</i>	<i>conv.</i>		
4.2	-28.111 00	-96.924 54	-0.333 73	-0.517 49	-0.517 54	-0.517 58	<i>conv.</i>	<i>conv.</i>	<i>conv.</i>		

^aAll calculations with $M \geq 500$ converged.

^b"*conv.*" denotes converged results, where increased M did not change the significant figures in the energy.

FIG. 11: Asymmetric dissociation of H_{50} : Relative errors in the correlation energies at MP2, CCSD, CCSD(T), and different LDMRG levels of theory (compared to the exact LDMRG results) in logarithmic scale.

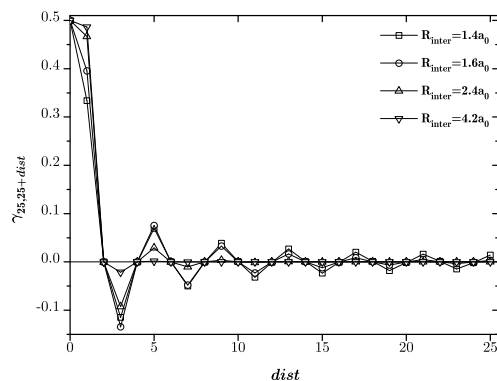


oscillations in the off-diagonal elements, while in the insulating regime (long R_{inter}) the off-diagonal elements decay much more rapidly. A similar picture is obtained from the density matrix during symmetric dissociation.

VI. CONCLUSIONS

We began this work with the question of how to describe nondynamic correlation in large systems, with the restriction that such systems are large in only one dimension. In our investigations, we have shown how the Density Matrix Renormalization Group (DMRG) provides a natural answer to this problem. The Matrix Product State that underlies the DMRG is a local, variational, size-consistent/size-extensive, and inherently mul-

FIG. 12: Asymmetric dissociation of H_{50} : Half-cross-section of the LDMRG α -one-particle density matrix at α -orbital no. 25.



tireference ansatz that can efficiently exploit the special structure of quasi-one-dimensional correlation. Using the intrinsic locality of the ansatz, we have formulated the *quadratic* scaling LDMRG algorithm, using only a straightforward screening criterion without the imposition of correlation domains. With this active space method, we could then obtain numerically exact solutions of the many-particle Schrödinger equation for all-trans-polyenes up to $C_{48}H_{50}$ (correlating the π_z -electrons) and hydrogen molecular chains up to $(H_2)_{50}$ (correlating 100 electrons in 100 orbitals).

By construction, a unique advantage of the LDMRG as compared to other local correlation methods, is its ability to capture nondynamic correlation. We can take advantage of locality in multireference problems so long as the correlation length is finite. We have demonstrated the capability and efficiency of the LDMRG in these situa-

tions by obtaining numerically exact correlation energies in the metal-to-insulator transition of linear H_{50} -chains, where we correlate 50 electrons in 50 orbitals.

With the possibility of accurately capturing nondynamic correlation in long molecules, we can now begin to address the quantitative description of strongly interacting states as found in the spectrum of materials such as the conjugated organic polymers. Here, the natural next step would be to combine an LDMRG description of the nondynamic correlation in the active π -space with our recent developments in Canonical Transformation Theory [60], to incorporate the dynamic correlation that arises in larger basis sets.

Acknowledgments

JH is funded by a Kekulé Fellowship of the Fond der Chemischen Industrie (Fund of the German Chemical Industry). GKC acknowledges support from Cornell University and the Cornell Center for Materials Research (CCMR). Computations were carried out in part on the Nanolab-Cluster of the Cornell NanoScale Science & Technology Facility (CNF), supported by NSF ECS 03-05765.

-
- [1] B. O. Roos, *Adv. Chem. Phys.* **69**, 399 (1987).
 [2] T. Van Voorhis and M. Head-Gordon, *Chem. Phys. Lett.* **317**, 575 (2000).
 [3] T. Van Voorhis and M. Head-Gordon, *J. Chem. Phys.* **112**, 5633 (2000).
 [4] T. Van Voorhis and M. Head-Gordon, *J. Chem. Phys.* **115**, 7814 (2001).
 [5] G. J. O. Beran, M. Head-Gordon, and S. R. Gwaltney, *J. Chem. Phys.* **124**, 114107 (2006).
 [6] D. Walter and E. A. Carter, *Chem. Phys. Lett.* **346**, 177 (2001).
 [7] D. Walter, A. Venkatnathan, and E. A. Carter, *J. Chem. Phys.* **118**, 8127 (2003).
 [8] A. Venkatnathan, A. B. Szilva, D. Walter, R. J. Gdanitz, and E. A. Carter, *J. Chem. Phys.* **120**, 1693 (2004).
 [9] B. D. Dunietz and R. A. Friesner, *J. Chem. Phys.* **115**, 11052 (2001).
 [10] G. E. Scuseria and P. Y. Ayala, *J. Chem. Phys.* **111**, 8330 (1999).
 [11] M. Schütz and H.-J. Werner, *Chem. Phys. Lett.* **318**, 370 (2000).
 [12] M. Schütz, *J. Chem. Phys.* **113**, 9986 (2000).
 [13] M. Schütz and H.-J. Werner, *J. Chem. Phys.* **114**, 661 (2001).
 [14] J. E. Subotnik and M. Head-Gordon, *J. Chem. Phys.* **123**, 064108 (2005).
 [15] P. Tavan and K. Schulten, *Phys. Rev. B* **36**, 4337 (1987).
 [16] K. Nakayama, H. Nakahano, and K. Hirao, *Int. J. Quantum Chem.* **66**, 157 (1998).
 [17] J. Lappe and R. J. Cave, *J. Phys. Chem. A* **104**, 2294 (2000).
 [18] M. Bockrath et al., *Nature* **397**, 598 (1999).
 [19] S. Belluci, J. Gonzalez, and P. Onorato, *Phys. Rev. Lett.* **95**, 186403 (2005).
 [20] J. Lee et al., *Phys. Rev. Lett.* **93**, 166403 (2004).
 [21] Z. Shuai, J. L. Brédas, S. K. Pati, and S. Ramasesha, *Proc. SPIE* **3145**, 293 (1997).
 [22] D. Yaron, E. E. Moore, Z. Shuai, and J. L. Brédas, *J. Chem. Phys.* **108**, 7451 (1998).
 [23] G. Fano, F. Ortolani, and L. Ziosi, *J. Chem. Phys.* **108**, 9246 (1998).
 [24] G. L. Bendazzoli, G. F. S. Evangelisti, F. Ortolani, and L. Ziosi, *J. Chem. Phys.* **110**, 1277 (1999).
 [25] A. O. Mitrushenkov, G. Fano, F. Ortolani, R. Linguerri, and P. Palmieri, *J. Chem. Phys.* **115**, 6815 (2001).
 [26] A. O. Mitrushenkov, R. Linguerri, P. Palmieri, and G. Fano, *J. Chem. Phys.* **119**, 4148 (2003).
 [27] S. R. White and R. L. Martin, *J. Chem. Phys.* **110**, 4127 (1999).
 [28] S. Daul, I. Ciofini, C. Daul, and S. R. White, *Int. J. Quantum Chem.* **79**, 331 (2000).
 [29] G. K.-L. Chan and M. Head-Gordon, *J. Chem. Phys.* **116**, 4462 (2002).
 [30] G. K.-L. Chan and M. Head-Gordon, *J. Chem. Phys.* **118**, 8551 (2003).
 [31] G. K.-L. Chan, *J. Chem. Phys.* **120**, 3172 (2004).
 [32] G. K.-L. Chan, M. Kállay, and J. Gauss, *J. Chem. Phys.* **121**, 6110 (2004).
 [33] G. K.-L. Chan and T. Van Voorhis, *J. Chem. Phys.* **122**, 204101 (2005).
 [34] Ö. Legeza, J. Röder, and B. A. Hess, *Mol. Phys.* **101**, 2019 (2003).
 [35] Ö. Legeza, J. Röder, and B. A. Hess, *Phys. Rev. B* **67**, 125114 (2003).
 [36] G. Moritz, B. A. Hess, and M. Reiher, *J. Chem. Phys.* **122**, 024107 (2005).
 [37] G. Moritz, A. Wolf, and M. Reiher, *J. Chem. Phys.* **123**, 184105 (2005).
 [38] G. Moritz and M. Reiher, *J. Chem. Phys.* **124**, 034103 (2006).
 [39] H. Ma, C. Liu, and Y. Jiang, *J. Chem. Phys.* **120**, 9316 (2004).
 [40] H. Ma, F. Cai, C. Liu, and Y. Jiang, *J. Chem. Phys.* **122**, 104909 (2005).
 [41] H. Ma, C. Liu, and Y. Jiang, *J. Chem. Phys.* **123**, 084303 (2005).
 [42] S. Östlund and S. Rommer, *Phys. Rev. Lett.* **75**, 3537 (1995).
 [43] S. Rommer and S. Östlund, *Phys. Rev. B* **55**, 2164 (1997).
 [44] F. Verstraete, D. Porras, and J. I. Cirac, *Phys. Rev. Lett.* **93**, 227204 (2004).
 [45] U. Schollwöck, *Rev. Mod. Phys.* **77**, 259 (2005).
 [46] E. R. Davidson, *J. Comp. Phys.* **17**, 87 (1975).
 [47] J. Catalán and J. L. G. de Paz, *J. Chem. Phys.* **120**, 1864 (2004).
 [48] T. D. Crawford et al., *Psi 3.2* (2003), see www.psiicode.org.
 [49] W. J. Hehre, R. F. Stewart, and J. A. Pople, *J. Chem. Phys.* **51**, 2657 (1969).

- [50] Basis sets were obtained from the Extensible Computational Chemistry Environment Basis Set Database, Version 02/25/04, as developed and distributed by the Molecular Science Computing Facility, Environmental and Molecular Sciences Laboratory which is part of the Pacific Northwest Laboratory, P.O. Box 999, Richland, Washington 99352, USA, and funded by the U.S. Department of Energy. The Pacific Northwest Laboratory is a multi-program laboratory operated by Battelle Memorial Institute for the U.S. Department of Energy under contract DE-AC06-76RLO 1830. Contact Karen Schuchardt for further information.
- [51] C. Angeli et al., DALTON, a molecular electronic structure program, release 2.0 (2005), see www.kjemi.uio.no/software/dalton/.
- [52] H.-J. Werner et al., MOLPRO, version 2002.6 (2002), a package of ab initio programs, see www.molpro.net.
- [53] G. K.-L. Chan, P. W. Ayers, and E. S. Croot, *J. Stat. Phys.* **109**, 289 (2002).
- [54] K. Okunishi, Y. Hieida, and Y. Akutsu, *Phys. Rev. E* **59**, R6227 (1999).
- [55] Ö. Legeza and G. FÁth, *Phys. Rev. B* **53**, 14349 (1996).
- [56] M. Takahashi and J. Paldus, *Phys. Rev. B* **31**, 5121 (1985).
- [57] J. Paldus, J. Čížek, and M. Takahashi, *Phys. Rev. A* **30**, 2193 (1984).
- [58] J. Paldus, M. Takahashi, and R. W. H. Cho, *Phys. Rev. B* **30**, 4267 (1984).
- [59] S. F. Boys, in *Quantum Theory of Atoms, Molecules and the Solid State*, edited by P. O. Löwdin, page 253, Academic, New York, 1968.
- [60] T. Yanai and G. K.-L. Chan, *J. Chem. Phys.* **124**, 194106 (2006).